

# Geometric Structure of Mutually Coupled Phase-Locked Loops

Hisao-Aki Tanaka, *Student Member, IEEE*, Shin'ichi Oishi, and Kazuo Horiuchi, *Fellow, IEEE*

**Abstract**—Dynamical properties such as lock-in or out-of-lock condition of mutually coupled phase-locked loops (PLL's) are problems of practical interest. The present paper describes a study of such dynamical properties for mutually coupled PLL's incorporating lag filters and triangular phase detectors. The fourth-order ordinary differential equation (ODE) governing the mutually coupled PLL's is reduced to the equivalent third-order ODE due to the symmetry, where the system is analyzed in the context of nonlinear dynamical system theory. An understanding as to how and when lock-in can be obtained or out-of-lock behavior persists, is provided by the geometric structure of the invariant manifolds generated in the vector field from the third-order ODE. In addition, a connection to the recently developed theory on chaos and bifurcations from degenerated homoclinic points is also found to exist. The two-parameter diagrams of the one-homoclinic orbit are obtained by graphical solution of a set of nonlinear (finite dimensional) equations. Their graphical results useful in determining whether the system undergoes lock-in or continues out-of-lock behavior, are verified by numerical simulations.

## I. INTRODUCTION

MUTUALLY COUPLED phase-locked loops (PLL's) are frequently used in practical communication systems to synchronize geographically separated timing clocks [1], [2]. The dynamical properties of such PLL's, e.g., their *lock-in* or *out-of-lock* conditions, present a problem of practical interest. Theoretical studies on *lock-in* condition have been carried out near the synchronized state [1], [2], while the dynamics occurring beyond this state has been recently studied in both single and mutually coupled PLL's [3]–[6]. When two PLL's are in the critical state where they are almost but not quite synchronized, chaotic phenomena can be experimentally and numerically observed for a wide range of realistic parameters [6]. Endo and Chua called this critical desynchronized state near the synchronization (*lock-in*) as the “marginal *out-of-lock* condition” in [6]. In the present paper, we elucidate the nature of such *marginality*, thereby establishing the limit of synchronization. To do so, we apply nonlinear dynamical systems theory to determine the geometric structure of the system-generated invariant manifolds.

Manuscript received May 10, 1994; revised October 11, 1995. This paper was recommended by Associate Editor M. Ogorzalek.

H.-A. Tanaka and S. Oishi are with the Department of Information and Computer Sciences, Waseda University, 3-4-1 Ohkubo, Shinjuku-ku, Tokyo, Japan.

K. Horiuchi is with the Department of Electronics and Communication Engineering, Waseda University, 3-4-1 Ohkubo, Shinjuku-ku, Tokyo, Japan.

Publisher Item Identifier S 1057-7122(96)03901-3.

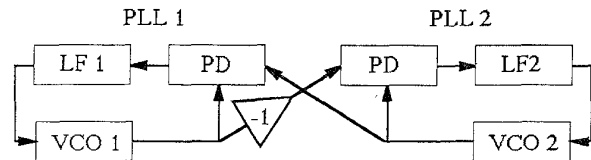


Fig. 1. Block diagram of considered mutually coupled PLL's.

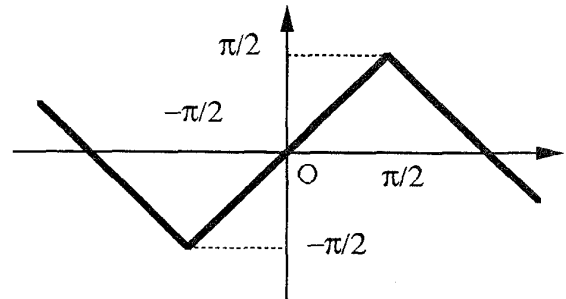


Fig. 2. Triangular characteristics of the phase detector.

## II. ORDER REDUCTION

Considered here are PLL's that incorporate a voltage-controlled oscillator (VCO), a phase detector (PD) having triangular characteristics (Fig. 1), and a loop filter (LF) comprising of a simple *RC* filter with transfer function  $F(S) = 1/(1+\tau S)$ , which is known as a lag filter. Fig. 2 shows a block diagram of the system, and the following fourth-order ordinary differential equation (ODE), the *phase model* [6], describes the dynamics of the phases

$$\begin{aligned} \ddot{\Phi}_1 + 2\zeta_1\dot{\Phi}_1 + h(\Phi_1 - \Phi_2) &= \delta, \\ \ddot{\Phi}_2 + 2\zeta_2\sqrt{\frac{r_1}{r_2}}\dot{\Phi}_2 + \left(\frac{r_1}{r_2}\right)h(\Phi_2 - \Phi_1) &= -\left(\frac{r_1}{r_2}\right)\delta \end{aligned} \quad (1)$$

where  $\Phi_1$  and  $\Phi_2$  are, respectively, the resultant phase of the output of VCO1 and VCO2 after subtracting  $\Omega t$ . Here,  $\Omega$  represents the synchronized angular frequency uniquely determined by the free-running angular frequencies of VCO1/VCO2 and the system parameters presented in [6].  $h$  is a  $2\pi$ -periodic triangular function (Fig. 1), while  $\zeta_1$ ,  $\zeta_2$ ,  $r_1$ ,  $r_2$ , and  $\delta$  are normalized parameters, respectively, defined as  $\zeta_1 = 1/2\sqrt{K_1\tau_1}$ ,  $\zeta_2 = 1/2\sqrt{K_2\tau_2}$ ,  $r_1 = K_2/K_1$ ,  $r_2 = \tau_2/\tau_1$ , and  $\delta = (\omega_{01} - \omega_{02})/(K_1 + K_2)$ , in which  $K_i$ ,  $\tau_i$ , and  $\omega_{0i}$  denote the total loop gain, loop filter time constant, and free-running angular frequency of PLL  $i$  ( $i = 1, 2$ ), respectively. Our goal in this section is to reduce (1) to the simplest equivalent ODE.

For this purpose, we first normalize (1) to give

$$\begin{aligned} \dot{q}_1 &= p_1 \\ \dot{q}_2 &= p_2, \\ \dot{p}_1 &= -\beta_1 h(q_1 - q_2) - \alpha_1 p_1 + \gamma_1 \\ \dot{p}_2 &= -\beta_2 h(q_2 - q_1) - \alpha_2 p_2 + \gamma_2 \end{aligned} \quad (2)$$

where  $q_1 = \Phi_1$ ,  $q_2 = \Phi_2$ ,  $\alpha_1 = 2\zeta_1$ ,  $\alpha_2 = 2\zeta_2\sqrt{r_1/r_2}$ ,  $\beta_1 = 1$ ,  $\beta_2 = r_1/r_2$ ,  $\gamma_1 = \delta$ , and  $\gamma_2 = -(r_1/r_2)\delta$ .

It should be noted that symmetry reduces (2) to a third-order ODE, namely, by introducing  $P_1 = p_1 + p_2$ ,  $P_2 = p_1 - p_2$ ,  $Q_1 = q_1 + q_2$ , and  $Q_2 = q_1 - q_2$ , (2) becomes

$$\dot{Q}_1 = P_1 \quad (3a)$$

$$\dot{Q}_2 = P_2 \quad (3b)$$

$$\dot{P}_1 = -\frac{\alpha_+ P_1 + \alpha_- P_2}{2} - \beta_- h(Q_2) + \gamma_+ \quad (3c)$$

$$\dot{P}_2 = -\frac{\alpha_- P_1 + \alpha_+ P_2}{2} - \beta_+ h(Q_2) + \gamma_- \quad (3d)$$

where  $\alpha_+ = \alpha_1 + \alpha_2$ ,  $\alpha_- = \alpha_1 - \alpha_2$ ,  $\beta_+ = \beta_1 + \beta_2$ ,  $\beta_- = \beta_1 - \beta_2$ ,  $\gamma_+ = \gamma_1 + \gamma_2$ , and  $\gamma_- = \gamma_1 - \gamma_2$ .

Note the solution for  $P_1$ ,  $P_2$ , and  $Q_2$  can only be determined by (3b)–(3d). In (3b)–(3d) there are two nonlinear terms  $-\beta_- h(Q_2)$  and  $-\beta_+ h(Q_2)$ . To reduce these two into one nonlinear term, we further employ the transformation  $x = P_1/\beta_- - P_2/\beta_+$ ,  $y = P_2/\beta_+$ , and  $z = Q_2$ , which reduces (3b)–(3d) to the following third-order ODE:

$$\begin{aligned} \dot{x} &= A_1 x + A_2 y, \\ \dot{y} &= B_0 + B_1 x + B_2 y - h(z), \\ \dot{z} &= \beta_+ y, \end{aligned} \quad (4)$$

where  $A_1 = (\alpha_- \beta_- - \alpha_+ \beta_+)/2\beta_+$ ,  $A_2 = (\beta_-/\beta_+ - \beta_+/\beta_-)\alpha_-/2$ ,  $B_0 = \gamma_-/\beta_+ = \delta$ ,  $B_1 = -\alpha_- \beta_-/2\beta_+$ , and  $B_2 = -(\alpha_- \beta_- + \alpha_+ \beta_+)/2\beta_+$ . Although  $h(z)$  can be either sinusoidal or triangular depending on the type of the employed phase detector, we only consider the triangular function here.

When transmission delays are incorporated into either phase equation (1) or (2), the same reduction can be carried out by applying some assumptions (See Appendix I).

### III. PIECEWISE-LINEAR ANALYSIS

Since (4) is  $2\pi$ -periodic with respect to  $z$ , let us concentrate on the region  $D = \{(x, y, z) | -\pi - \delta \leq z \leq \pi - \delta\}$  in order to examine the geometric structure of the defined vector field. Region  $D$  can be divided into three segments:  $D_+$ ,  $D_0$ , and  $D_-$ , respectively, defined by  $D_+ = \{(x, y, z) | \pi/2 < z \leq \pi - \delta\}$ ,  $D_0 = \{(x, y, z) | |z| \leq \pi/2\}$ , and  $D_- = \{(x, y, z) | -\pi - \delta < z < -\pi/2\}$ , where the vector field in each segment is linear. Further, denote the planes  $\{(x, y, z) | z = \pm\pi/2\}$  as  $\Sigma_+$ , and  $\Sigma_-$ , respectively. From (4) and the form of  $h(z)$ , it follows that unique equilibrium points at  $O_+$ ,  $O_0$ ,  $O_-$  exists in  $D_+$ ,  $D_0$ ,  $D_-$ , with their positions being, respectively,

$$O_{\pm} = (0, 0, \pm\pi - \delta), \quad O_0 = (0, 0, \delta). \quad (5)$$

It should be noted that  $O_+$  and  $O_-$  can be identified if we consider the vector field is defined on the cylinder  $R^2 \times S^1 = \{(x, y, z) | (x, y) \in R^2, z \in S^1\}$ .

Our attention is focused on the following three sets of chaotic parameters experimentally obtained by Endo and Chua [6]:

#### 1) Asymmetric high damping [Case 1)]

$$\zeta_1 = 0.614, \quad \zeta_2 = 0.331$$

$$f_{01} = 18\,250 \text{ Hz}, \quad f_{02} = 25\,400 \text{ Hz}$$

$$r_1 = 45\,500/12\,500, \quad r_2 = 5.027/5.298$$

$$\delta \equiv 2\pi f_{01} - f_{02}/45\,500 + 12\,500, = -0.774\,565. \quad (6)$$

#### 2) Symmetric high damping [Case 2)]

$$\zeta_1 = 0.614, \quad \zeta_2 = 0.618$$

$$f_{01} = 17\,000 \text{ Hz}, \quad f_{02} = 27\,818 \text{ Hz}$$

$$r_1 = 43\,300/12\,500, \quad r_2 = 1.480/5.298$$

$$\delta \equiv 2\pi f_{01} - f_{02}/43\,300 + 12\,500, = -1.218\,127. \quad (7)$$

#### 3) Symmetric low damping [Case 3)]

$$\zeta_1 = 0.0914, \quad \zeta_2 = 0.0964$$

$$f_{01} = 22\,450 \text{ Hz}, \quad f_{02} = 23\,183 \text{ Hz}$$

$$r_1 = 12\,440/12\,200, \quad r_2 = 2.16/2.45$$

$$\delta \equiv 2\pi f_{01} - f_{02}/12\,440 + 12\,200, = -0.186\,914. \quad (8)$$

The following parameter sets are, respectively, obtained for Cases 1)–3):

$$A_1 = -1.242519, \quad A_2 = -0.037\,054$$

$$B_1 = -0.019\,424, \quad B_2 = -1.281\,369$$

$$B_0 = \delta = -0.774\,565, \quad \beta_+ = 4.836\,228 \quad (9)$$

$$A_1 = -1.460\,438, \quad A_2 = -0.502\,870$$

$$B_1 = -1.353\,398, \quad B_2 = -4.167\,234$$

$$B_0 = \delta = -1.218\,127, \quad \beta_+ = 13.686\,562 \quad (10)$$

$$A_1 = -0.194\,297, \quad A_2 = -0.168\,230$$

$$B_1 = -0.000\,891, \quad B_2 = -0.196\,079$$

$$B_0 = \delta = -0.186\,914, \quad \beta_+ = 2.156\,572. \quad (11)$$

These parameter sets, respectively, correspond to the real eigenvalues  $\lambda_s$ ,  $\lambda_{ss}$ , and  $\lambda_u$  of the linearized matrix of the vector fields at  $O_+$  and  $O_-$ , which are obtained by solving

$$-\lambda(\lambda - A_1)(\lambda - B_2) + \beta_+(A_1 - \lambda) + A_2 B_1 \lambda = 0 \quad (12)$$

giving  $(\lambda_s, \lambda_{ss}, \lambda_u) = (-1.242\,336, -2.931\,525, 1.649\,973)$  for (9),  $(\lambda_s, \lambda_{ss}, \lambda_u) = (-1.405\,973, -6.432\,011, 2.210\,312)$  for (10), and  $(\lambda_s, \lambda_{ss}, \lambda_u) = (-0.194\,283, -1.569\,894, 1.373\,800)$  for (11). In segment  $D_0$ , the real eigenvalue  $\lambda_1$  and the pair of complex-conjugate eigenvalues  $\lambda_{2,3}$  are obtained by

$$-\lambda(\lambda - A_1)(\lambda - B_2) + \beta_+(\lambda - A_1) + A_2 B_1 \lambda = 0 \quad (13)$$

giving  $(\lambda_1, \lambda_{2,3}) = (1.242\,706, -0.640\,591 \pm 2.103\,602i)$  for (9),  $(\lambda_1, \lambda_{2,3}) = (-1.571\,786, -2.027\,943 \pm 2.933\,330i)$  for (10), and  $(\lambda_1, \lambda_{2,3}) = (-0.194\,310, -0.098\,033 \pm 1.465\,200i)$  for (11). The corresponding eigenvectors  $e_u$ ,  $e_s$ ,  $e_{ss}$ ,  $e_1$ , and  $e_{2,3}$  to the above eigenvalues determine the invariant manifolds  $W^s(O_-)$ ,  $W_r^s(O_0)$ ,  $W_c^s(O_0)$ , and

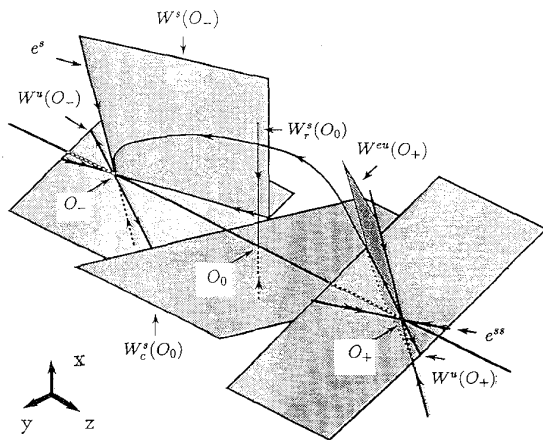


Fig. 3. Saddle connection in piecewise-linear vector field. Generically,  $W^u(O_+)$  becomes tangent to the weakly stable direction ( $e^s$  in this case) after extended onto  $W^s(O_-)$ .  $W_r^s(O_0)$  and  $W_c^s(O_0)$ , respectively, denotes the eigenspaces of the real eigenvalue and the complex conjugate eigenvalues at  $O_0$ .

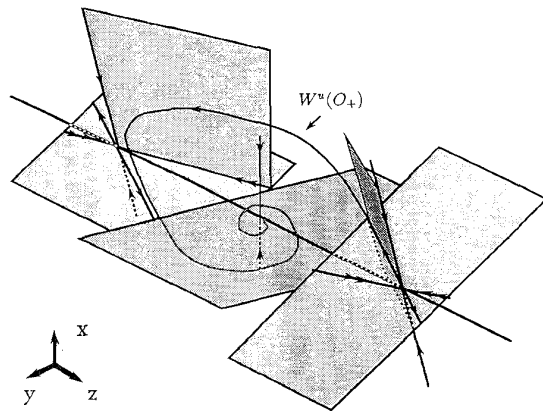


Fig. 4. Lock-in dynamics for  $\delta > \delta_c$ .  $W^u(O_+)$  is extended eventually to  $O_0$  (the lock-in state). Lock-in can be obtained from almost all initial conditions.

$W^u(O_{\pm})$ , as well as the extended unstable manifold  $W^{eu}(O_+)$ , where  $W^{eu}(O_+)$  is tangent at  $O_+$  to the linear space spanned by  $e^u$  and  $e^s$  (see [7] which proves the existence of such an invariant manifold).  $W^s$  and  $W^u$ , respectively, represent the stable manifold and the unstable manifold. Fig. 3 schematically depicts these invariant manifolds. From (5), (12), and (13), it is evident that the positions of  $O_+$ ,  $O_0$ , and  $O_-$  depend only on the parameter  $\delta$ , and that the eigenvalues (vectors) are not dependent on  $\delta$ . Hence, if we only change  $\delta$ , i.e., the free-running angular frequency  $f_{02}$  of PLL 2, then  $W^s(O_-)$ ,  $W_r^s(O_0)$ ,  $W_c^s(O_0)$ ,  $W^u(O_{\pm})$ , and  $W^{eu}(O_+)$  do not change their normal vectors or directions, though they are shifted in the  $z$ -direction by the position changes of  $O_-$ ,  $O_+$ , and  $O_0$ . Therefore, a critical parameter  $\delta_c$  is expected to exist under the following situation: 1)  $p_+$  is mapped onto the intersection of  $W^s(O_-)$  and  $\Sigma_-$  by the linear flow in  $D_0$  for  $\delta = \delta_c$  (Fig. 3). If  $\delta \neq \delta_c$ , the following situations are expected to occur depending on whether  $\delta > \delta_c$  or  $\delta < \delta_c$ : 2)  $p_+$  is mapped to the left of  $W^s(O_-)$  on  $\Sigma_-$  for  $\delta > \delta_c$

(Fig. 4) or 3)  $p_+$  is mapped to the right of  $W^s(O_-)$  for  $\delta < \delta_c$  (Fig. 5), where  $p_+$  denotes the intersection of the plane  $\Sigma_+$  and the unstable manifold  $W^u(O_+)$ . Situation 1) leads to a set of two nonlinear (finite dimensional) equations derived as shown in Appendix II where the values of  $f_{02}$  and  $T$  are unknown. By using the parameter values of  $f_{01}$ ,  $\zeta_{1,2}$ , and  $r_{1,2}$  in (9)–(11), the critical parameter  $\delta_c$  (the critical free-running angular frequency  $\tilde{f}_{02}$ ) for situation 1) can be obtained by solving this set of nonlinear equations, respectively, giving

$$\tilde{T} = 0.787078$$

and

$$\tilde{f}_{02} = 25\,390.248,$$

i.e.,

$$\delta_c = -0.773\,508 \quad (14)$$

for (9),

$$\tilde{T} = 0.614\,754$$

and

$$\tilde{f}_{02} = 27\,811.590$$

i.e.,

$$\delta_c = -1.217\,405 \quad (15)$$

for (10), and

$$\tilde{T} = 1.075\,136,$$

and

$$\tilde{f}_{02} = 23\,181.330$$

i.e.,

$$\delta_c = -0.186\,488 \quad (16)$$

for (11), where  $T$  is the time interval  $p_+$  being mapped from  $\Sigma_+$  to  $\Sigma_-$ . When  $\delta = \delta_c$ , the point mapped from  $p_+$  to the intersection of  $W^s(O_-)$  and  $\Sigma_-$  asymptotically goes to  $O_-$  because  $\lambda_{ss} < \lambda_s < 0$ ; being a situation that indicates a saddle connection (a homoclinic orbit in this case) exists between  $O_+$  and  $O_-$  as shown in Fig. 3. When  $\delta$  is slightly larger than  $\delta_c$ , the orbits from the neighborhood of  $p_+$  go to the sink  $O_0$ , i.e., the two PLL's undergo lock-in from their broad initial states (Fig. 4). However, when  $\delta$  is slightly less than  $\delta_c$ , being the case if the set of parameters are per (9)–(11), then the point mapped from  $p_+$  on  $\Sigma_-$  is on the other side of  $O_0$  with respect to  $W^s(O_-)$ . Such a situation can be considered to lead to the loss of the global lock-in because  $W^{eu}(O_+)$  on  $\Sigma_-$  (Fig. 5) prevents most initial points from reaching the sink  $O_0$ . Adding to this lock-in mechanism, the homoclinic orbit at (14) in Case 1) is shown to appear near a degenerated homoclinic point—orbit-flip homoclinic point [8]–[10]—at which the homoclinic orbit is doubly asymptotic to the strongly stable direction  $e^{ss}$  and the unstable direction  $e^u$  at the saddle [11]. Kokubu and Oka [12] demonstrated the existence of the Smale horseshoe and the invariant foliation in an unfolding of the orbit-flip homoclinic point, while the resultant chaotic phenomena near the orbit-flip homoclinic point is reported in [11]. Homburg, Kokubu, and Krupa also demonstrated the Smale horseshoe generation in another degenerated homoclinic point—inclination-flip homoclinic point [10]—at which the

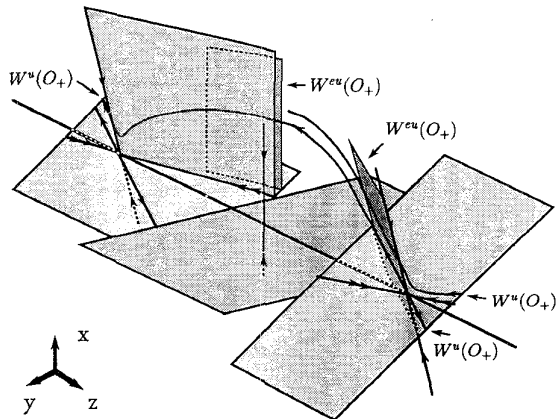


Fig. 5. *Out-of-lock* dynamics for  $\delta < \delta_c$ . Most initial conditions in the positive  $y$  region or in the neighborhood of  $O_0$  eventually go to  $O_0$ , while solutions starting from initial conditions away from  $O_0$  in the negative  $y$  region exhibit *out-of-lock* persistently.

invariant manifolds  $W^{eu}$  and  $W^s$  become tangent along the homoclinic orbit [13]. The inclination-flip homoclinic point and the resultant dynamics in (4) will be reported in the future.

#### IV. BRANCH OF A HOMOCLINIC ORBIT

As mentioned in the previous section, a saddle connection, in this case a one-homoclinic orbit, appears at  $\delta_c$ ; beyond which global *lock-in* of the two PLL's is lost. Such one-homoclinic orbit forms a submanifold of codimension one in the parameter space (see Theorem 3.5.1 in [10], p. 399), namely, a one dimensional homoclinic branch in a suitable two-parameter space. Here, we consider a set of two practical parameters  $f_{02}$  and  $K_2$ , for which a one-homoclinic branch can be computed by solving the set of two nonlinear equations contained in Appendix II for various values of  $K_2$ . Fig. 6 shows the computed one-homoclinic branch (dotted by  $\diamond$ ) in the  $(f_{02}, K_2)$ -parameter space for Case 1). The ones for Cases 2) and 3), respectively, exhibit a similar characteristics between  $K_2$  and  $f_{02}$  as in Fig. 6. Namely, the critical  $f_{02}$  value is almost linearly proportional to  $K_2$  in the practical range of  $K_2$ . These linear characteristics observed in Fig. 6 seem to coincide with the experimental facts observed in a practical range of parameter  $K_2$  values. Employing the fourth-order Runge-Kutta integration scheme with the time step 0.01 and setting certain (wide range of) initial states away from the synchronized states in (4), the critical change of dynamics is verified at the various sets of parameters dotted by  $+$  and  $\square$  in Fig. 6. The insets of Fig. 6 show the typical solutions in the corresponding dynamics projected to the  $(y, z)$ -plane.

#### V. CONCLUSION

We presented theoretical and numerical results that explain experimental results of mutually coupled PLL's in the critical state between *lock-in* and *out-of-lock* dynamics. Such critical state, namely, the limit of capture/lock dynamics is now considered to be the onset of the homoclinic orbit. For three typical, realistic parameter sets, the one dimensional homoclinic bifurcation set in the  $(f_{02}, K_2)$ -parameter space is obtained

by solving the nonlinear equations defining a homoclinic orbit. Numerical simulations show a good agreement to the expected critical change of dynamics for various parameters in the neighborhood of the one-homoclinic branches.

#### APPENDIX I TRANSMISSION DELAYS

This Appendix describes the reduction of the phase model (1) or (2) which incorporates transmission delays. We consider a system of two mutually coupled PLL's incorporating transmission delays of the signals between two PLL's and the corresponding estimates of these delays—a system employing the so-called delay line compensation technique [2]. The governing equation of the phase differences for such a system that incorporates a loop filter whose transfer function  $F(s) = 1/(1 + \tau S)$  can be written as follows:

$$\begin{aligned} \ddot{\Phi}_1(t) + 2\zeta_1 \dot{\Phi}_1(t) + h[\Phi_1(t - \tau_{12}) - \Phi_2(t - \hat{\tau}_{12})] &= \delta \\ \ddot{\Phi}_2(t) + 2\zeta_2 \sqrt{\frac{r_1}{r_2}} \dot{\Phi}_2(t) + \left(\frac{r_1}{r_2}\right) & \\ h[\Phi_2(t - \tau_{21}) - \Phi_1(t - \hat{\tau}_{21})] &= -\left(\frac{r_1}{r_2}\right) \delta \end{aligned} \quad (17)$$

where  $\tau_{ij}$  denotes the delay of signals traveling from PLL  $j$  to PLL  $i$ , while;  $i, j = 1, 2; i \neq j$ .  $\hat{\tau}_{ij}$  denotes the estimate of  $\tau_{ij}$  for delay compensation;  $i, j = 1, 2; i \neq j$ . It is noted that (17) becomes (1) in case  $\tau_{12} = 0, \hat{\tau}_{12} = 0, \tau_{21} = 0,$  and  $\hat{\tau}_{21} = 0$ . If  $\tau_{ij} = \hat{\tau}_{ij}$  hold,  $P_1 = \dot{\Phi}_1 + \dot{\Phi}_2, P_2 = \dot{\Phi}_1 - \dot{\Phi}_2, Q_1 = \Phi_1 + \Phi_2,$  and  $Q_2 = \Phi_1 - \Phi_2,$  transform (17) to

$$\dot{Q}_1 = P_1 \quad (18a)$$

$$\dot{Q}_2 = P_2, \quad (18b)$$

$$\dot{P}_1 = -\frac{\alpha_+ P_1 + \alpha_- P_2}{2} - \beta_+ h[Q_2(t - \tau_{12})] + \gamma_+ \quad (18c)$$

$$\dot{P}_2 = -\frac{\alpha_- P_1 + \alpha_+ P_2}{2} - \beta_- h[Q_2(t - \tau_{21})] + \gamma_- \quad (18d)$$

for which the solution for  $P_1, P_2,$  and  $Q_2$  can only be determined by (18b)–(18d). In addition, when  $\tau_{ij} = \tau_{ji} = \tau$  holds, the transformation  $x = P_1/\beta_- - P_2/\beta_+, y = P_2/\beta_+ m$  and  $z = Q_2,$  reduces (18) to the following differential-difference equation:

$$\begin{aligned} \dot{x} &= A_1 x + A_2 y \\ \dot{y} &= B_0 + B_1 x + B_2 y - h[z(t - \tau)] \\ \dot{z} &= \beta_+ y, \end{aligned} \quad (19)$$

in which the time delay  $\tau$  appears only in  $h$ .

#### APPENDIX II NONLINEAR EQUATION FOR A HOMOCLINIC ORBIT

This Appendix describes the derivation of the finite dimensional nonlinear equations that determine  $T$  and  $f_{02}$  of the homoclinic orbit for given parameters. A saddle connection—a homoclinic orbit—exists when  $p_+$  is mapped by the linear flow

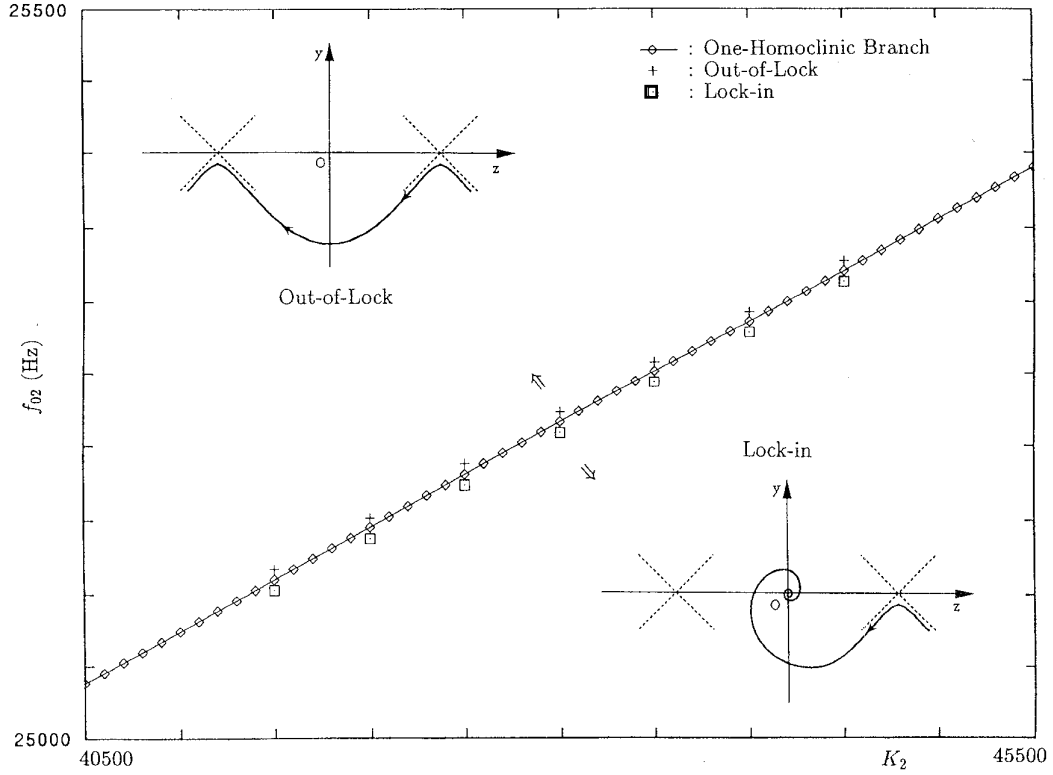


Fig. 6. One-homoclinic bifurcation set for Case (1) in the  $(f_{02}, K_2)$ -parameter space. Two insets show the *lock-in* (observed at  $\square$ ) and the *out-of-lock* dynamics (at  $+$ ) projected to the  $(y, z)$ -plane, respectively. This bifurcation set also presents the limit of synchronization between the two PLL's.

in  $D_0$  onto the line defined by  $W^s(O_-) \cap \Sigma_-$ , as in Fig. 2. Such a situation leads the following two conditions on  $T$  and  $f_{02}$ :

- 1)  $\Psi(p_+)$  is located on  $W^s(O_-)$ , where  $\Psi$  is a flow-defined map from  $\Sigma_+$  to  $\Sigma_-$ . (Cond. 1);
- 2) From the definition of  $\Psi$ , the  $z$  element of  $\Psi(p_+)$  equals to  $-\pi/2$ . (Cond. 2).

Since the flow in  $D_+$  is linear,  $W^u(O_+)$  becomes a line. This leads the exact position of  $p_+$ , i.e., the intersection of  $W^u(O_+)$  and  $\Sigma_+$

$$\begin{aligned} p_+ &= (x, y, z) \\ &= \left[ A_2(\lambda_u - A_1)^{-1} \beta_+^{-1} \left( \frac{\delta - \pi}{2} \right) \lambda_u, \right. \\ &\quad \left. \beta_+^{-1} \left( \frac{\delta - \pi}{2} \right) \lambda_u, \frac{\pi}{2} \right]. \end{aligned} \quad (20)$$

Similarly,  $W^s(O_-)$  becomes a plane spanned by  $e_s$  and  $e_{ss}$  at  $O_-$ , satisfying the following equation:

$$\begin{aligned} W^s(O_-) : & \beta_+(\lambda_s - \lambda_{ss}) \left( \frac{1 - A_1}{\lambda_s} \right) \left( \frac{1 - A_1}{\lambda_{ss}} \right) x \\ & - A_1 A_2 \beta_+ \left( \frac{1}{\lambda_{ss}} - \frac{1}{\lambda_s} \right) y \\ & + A_2(\lambda_{ss} - \lambda_s)(z + \pi + \delta) = 0. \end{aligned} \quad (21)$$

To obtain  $\Psi$ , we transform the original coordinate  $(x, y, z)$  in  $D_0$  to a canonical coordinate  $(X, Y, Z)$  by the following

transformations

$$(x, y, z)^T \rightarrow (x, y, \hat{z})^T = (x, y, z - \delta) \quad (22)$$

$$(x, y, \hat{z}) \rightarrow Q(X, Y, Z)^T \quad (23)$$

where  $Q$  is given as

$$Q = \begin{bmatrix} \frac{f_1}{\beta_+} & \frac{-f_2}{\beta_+} & \frac{A_2 \lambda_1}{(\lambda_1 - A_1) \beta_+} \\ \frac{\sigma}{\beta_+} & \frac{-\omega}{\beta_+} & \frac{\lambda_1}{\beta_+} \\ 1 & 0 & 1 \end{bmatrix} \quad (24)$$

in which  $f_1$  and  $f_2$  are given by

$$f_1 + i f_2 = \frac{A_2(\sigma + \omega i)(\sigma - A_1 - \omega i)}{(\sigma - A_1)^2 + \omega^2} \quad (25)$$

where  $\sigma, \omega$  denotes the real and imaginary parts of  $\lambda_2$ , respectively. Equations (22) and (23) lead to the following expression of  $\Psi$

$$\Psi(p_+) = Q J Q^{-1} \hat{p}_+ + (0, 0, \delta)^T \quad (26)$$

where  $\hat{p}_+ = p_+ - (0, 0, \delta)^T$ , and  $J$  is given as

$$J = \begin{bmatrix} \exp(\sigma T) \cos \omega T & -\exp(\sigma T) \sin \omega T & 0 \\ \exp(\sigma T) \sin \omega T & \exp(\sigma T) \cos \omega T & 0 \\ 0 & 0 & \exp(\lambda_1 T) \end{bmatrix}. \quad (27)$$

Combining (20), (21), (24), (26), and (27), Cond. 1, and Cond. 2 lead to a set of two nonlinear equations in the unknowns  $T$

and  $f_{02}$ , which can be solved via Newton's method. Such computation for a saddle connection has been previously carried out in [4] for the second-order piecewise-linear ODE.

#### ACKNOWLEDGMENT

The authors would like to thank Professor T. Endo of Meiji University for providing us the experimental data. One of the authors (H. Tanaka) would like to thank Professor T. Endo, Meiji University, T. Matsuda, NTT Transmission Systems Laboratories, and Dr. S. Watanabe, Niels Bohr Institute for constructive comments and discussions. Also, he acknowledges Assistant Professor R. Tokunaga, Tsukuba University for providing him a useful reference [10].

#### REFERENCES

- [1] H. Inose, H. Fujisaki, and T. Saito, "Theory of mutually synchronized systems," *Electron. Commun. Japan.*, vol. 49, no. 4, pp. 755–763, Apr. 1966.
- [2] K. Dessouky and W. C. Lindsey, "Phase and frequency transfer between mutually synchronized oscillators," *IEEE Trans. Commun.*, vol. 32, pp. 110–117, Feb. 1984.
- [3] T. Endo and L. O. Chua, "Chaos from phase-locked loops," *IEEE Trans. Circuits Syst.*, vol. 35, no. 8, pp. 987–1003, Aug. 1988.
- [4] ———, "Piecewise-linear analysis of high-damping chaotic phase-locked loops using Melnikov's method," *IEEE Trans. Circuit Syst.*, vol. 40, pp. 801–807, Nov. 1993.
- [5] E. Bradley, "Using chaos to broaden the capture range of a phase-locked loop," *IEEE Trans. Circuits Syst.*, vol. 40, pp. 808–818, Nov. 1993.
- [6] T. Endo and L. O. Chua, "Chaos from two-coupled phase-locked loops," *IEEE Trans. Circuits Syst.*, vol. 37, pp. 1183–1187, Sept. 1990.
- [7] M. Hirsch, C. Pugh, and M. Shub, *Invariant Manifolds*. Berlin: Springer-Verlag, 1977, LNM583.
- [8] K. Iori, E. Yanagida, and T. Matsumoto, " $N$ -homoclinic bifurcations of piecewise-linear vector fields," in *Structure and Bifurcations of Dynamical Systems*, S. Ushiki, Ed. Singapore: World Scientific, (Advanced Series in Dynamical Systems), 1993, vol. 11, pp. 82–97.
- [9] M. Kisaka, H. Kokubu, and H. Oka, "Bifurcations to  $N$ -homoclinic orbits and  $N$ -periodic orbits in vector fields," *J. Dynam. Diff. Eq.*, vol. 5, pp. 305–357, 1993.
- [10] T. Matsumoto, M. Komuro, H. Kokubu, and R. Tokunaga, *Bifurcations*. Tokyo: Springer-Verlag, 1993.
- [11] H. Tanaka, "Chaos from orbit-flip homoclinic orbits generated in a practical circuit," *Phys. Rev. Lett.*, vol. 70, pp. 1339–1342, Feb. 1995.
- [12] H. Kokubu and H. Oka, (in preparation).
- [13] A. J. Homburg, H. Kokubu, and M. Krupa, "The cusp horseshoe and its bifurcations in the unfolding of an inclination-flip homoclinic orbit," *J. Ergod. Th.*, vol. 14, no. 4, pp. 667–693, 1994.



**Hisa-Aki Tanaka** (S'94) received the B.E. degree in electrical engineering, the M.E. and D.E. degrees in electronics and communication engineering, from Waseda University, Tokyo, Japan, respectively, in 1990, 1992, and 1995.

Since 1995, he has been a Visiting Research Fellow at the University California, Berkeley. His current research interests are in the interdisciplinary area of communication systems, biology, and nonlinear physics.

Dr. Tanaka has received the 1995–1996 Research Fellowships of the Japan Society for the Promotion of Science for Young Scientists. He is a member of the Institute of Electronics, Information, and Communication Engineers (IEICE) and Physical Society of Japan.



**Shin'ichi Oishi** was born in Japan on May 9, 1953. He received the B.E., M.E., and D.E. degrees, all in electronics and communication engineering, from Waseda University Tokyo, Japan, in 1976, 1978, and 1981, respectively.

In 1980, he joined the faculty of the School of Science and Engineering, Waseda University. Since then he has engaged in education and research in the fields of nonlinear science, applied mathematics, and numerical analysis. He is now a Professor with the Department of Information and Computer Sciences.

Dr. Oishi was the Editor of the IEICE TRANSACTIONS ON FUNDAMENTALS during 1993–1994. He received Best Paper Awards in 1992 and 1995 from IEICE.



**Kazuo Horiuchi** (SM'83–F'90) was born in Japan on January 7, 1929. He received the B.E., M.E., and D.E. degrees, all in electrical communication engineering, from Waseda University Tokyo, Japan, in 1952, 1954, and 1958, respectively.

In 1957, he joined the faculty of the School of Science and Engineering, Waseda University, and since then, as a faculty member, he has been engaged in education and research in the fields of electromagnetic wave theory, information and communication theory, circuit and system theory,

applied mathematics, and others. He is now a Professor with the Department of Electronics and Communication Engineering. Recently, he is particularly interested in studying the functional analysis of nonlinear systems, including nonlinear wave propagation. He is also an author of the books: *Mathematics for Electrical Engineering*, *Electromagnetic Theory*, *Applied Analysis*, and *A Course of Applied Mathematics*.

Dr. Horiuchi is the President of IEICE, the Chairperson of the Executive Committee of the Symposia on Nonlinear Theory and Its Applications (NOLTA), and a Member of the Science Council of Japan. He was a President of the Society of Information Theory and Its Applications, and a Vice-President, a Director, the first Chairperson of Engineering Sciences Group and the first Editor-in-Chief of the IEICE. He received the Distinguished Services Award in 1990, the Achievement Award in 1981 and the Best Paper Award in 1994 from IEICE.